Energy Advances

Accepted Manuscript

This article can be cited before page numbers have been issued, to do this please use: J. Zhang, R. Knibbe and I. Gentle, *Energy Adv.*, 2024, DOI: 10.1039/D4YA00420E.

ROYAL SOCIETY OF CHEMISTRY

rsc.li/energy-advances

View Article Online
DOI: 10.1039/D4YA00420E

ARTICLE

Triethanolamine-assisted surface reconstruction of nickel oxide for efficient oxygen evolution reaction

Received 00th January 20xx,
Accepted 00th January 20xx

DOI: 10.1039/x0xx00000x

Jiayun Zhang,[a] Ruth Knibbe* [b] and Ian Gentle* [a]

Developing low cost and highly efficient electrocatalysts for oxygen evolution reaction (OER) is highly desired for the renewable energy production. Ni-based electrocatalysts have been widely investigated as candidates for OER, but developing a low-cost, easily synthesized electrocatalyst with high activity and good stability remains elusive. Herein, we report the facile electrodeposition of triethanolamine-decorated Ni oxide on carbon paper (Ni/CP-TEA) as an efficient electrocatalyst for water oxidation. Structural and experimental analyses reveal that the electrode surface is modified by triethanolamine (TEA) through Ni-N coordination bonding. The leaching of TEA drives rapid *in-situ* surface reconstruction, facilitating the generation of high-valence Ni (Ni^{3+}) species, thereby accelerating the OER performance. The Ni/CP-TEA exhibits enhanced electrocatalytic OER performance with a low overpotential of 320 mV at 10 mA·cm^{-2} and good long-term stability. This work presents a simple route for the rational design of cost-effective and highly efficient OER catalysts.

Introduction

Renewable energy sources are crucial for meeting growing energy demands and addressing environmental concerns.[1, 2] Among the many emerging technologies, electrocatalytic water splitting stands out as an efficient process for green hydrogen production.[3, 4] However, the oxygen evolution reaction (OER), a key component of water splitting, suffers from intrinsically sluggish kinetics, limiting the efficiency and practical application of water electrolysis. To date, Ru/Ir-based oxides are the benchmark OER electrocatalysts,[5, 6] however their cost, scarcity and unsatisfactory durability have hindered their widespread application.[7] Significant efforts have been devoted to developing highly efficient and cost-effective OER electrocatalysts.[8-10]

Earth-abundant Ni-based oxides have received considerable interest because of their promising OER performance and stability.[11-18] However, the catalytic mechanism of Ni-based OER catalysts remains a topic of scientific debate.[19] It has been demonstrated that during OER under alkaline conditions, the surfaces of numerous transition-metal based catalysts including chalcogenides, nitrides, and phosphides undergo phase transition and reconstruction processes, transforming into the corresponding oxides.[20-23] Generally, these *in situ*-generated higher valence oxide species display enhanced activities [21, 22] and are regarded as one of the reasons for the excellent catalytic activity.[24, 25] Therefore, more efforts to explore surface reconstruction and understand the catalytic origins are essential for the rational design of OER electrocatalysts.

Although binary or ternary metal-based compounds, such as S-FeCoNi LDH,[26] N-$NiMoO_4$[27] and Fe–NiSOH[25] and others have been investigated, the structural complexity of these materials makes it difficult to gain a deeper mechanistic understanding. Also, strategies for fabricating these materials – including hydrothermal, solvothermal, and chemical vapor deposition synthesis methods – are complex and/or require high energy. A simple and effective synthesis strategy for a low-cost efficient electrocatalyst with high stability is desired.

Metal coordination complexes have received extensive attention as a class of OER electrocatalysts. It has been demonstrated that organic ligands can be electrochemically extracted under anodic potential, leaving the inorganic oxides as the active species.[28] For example, Ni complexes can rapidly generate active NiOx species under an oxidation voltage.[29] The tannin-NiFe complex film on carbon fiber paper showed much larger mass activity compared to NiFe double layered hydroxide (LDH). The organic ligand tannic acid in tannin-NiFe was extracted under anodic potential, leaving behind $Ni_xFe_{1-x}O_yHz$ as the OER-active species.[28] If the surface of Ni oxides is modified with a complex agent which can be easily removed under anodic potential, it could potentially facilitate the surface reconstruction process and promote the formation of high valence Ni species for OER. Triethanolamine (TEA) functions as a ligand that is frequently used as a precipitant in the synthesis of Ni-based LDH electrocatalysts, along with other compounds.[30-32] During sample preparation, TEA can also help modify the catalysts' morphology.[31, 33] When introduced to the electrolyte in the electrodeposition process, TEA may modulate the morphology through forming Ni-complexes which have a different deposition rate to the Ni ions. Additionally, TEA may coordinate with Ni through its N group and remain on the

[a] School of Chemistry and Molecular Biosciences, The University of Queensland, Brisbane, QLD 4072, Australia.
[b] School of Mechanical and Mining Engineering, The University of Queensland, Brisbane, QLD 4072, Australia.
† Electronic Supplementary Information (ESI) available: See DOI: 10.1039/x0xx00000x

surface after synthesis, potentially enhancing the oxidation and reconstruction process under oxidation potential.

In the present work, we prepared a TEA-modified Ni oxide (Ni/CP-TEA) electrocatalyst, introducing Ni-N coordination that influences both the morphology and chemical structure of the electrocatalyst, which exhibits efficient OER activity. Structural and activity analysis of both fresh and post-reaction samples reveals that the TEA modifies the morphology and induces increased active surface area. The leaching of the TEA from the surface accelerates the *in-situ* surface reconstruction process and promotes the generation of higher valence Ni species, thereby enhancing the OER performance.

Experimental

Chemical and materials

$NiSO_4 \cdot 6H_2O$ (>99%) and triethanolamine (TEA) were purchased from Sigma-Aldrich and used as received. Potassium hydroxide (99% KOH, analytical grade, Fe content < 0.0003%) were purchased from Chem-Supply Pty Ltd. Carbon paper (CP, AvCarb carbon paper (P50)) were obtained from Fuel Cell Store.

Preparation of Ni/CP-TEA and Ni/CP

Carbon paper (CP) was first cut into 1 × 1 cm pieces and subsequently treated in an oven at 250°C for 2 h under Ar. Then the CP was ultrasonically cleaned in ethanol and deionized (DI) water for 10 min, respectively, and dried in an oven at 50°C overnight. As shown in Scheme 1, the samples were synthesized using electrodeposition. The deposition electrolyte was prepared by dissolving $NiSO_4 \cdot 6H_2O$ (0.1 M) and TEA (5 mM) into 30 mL DI water. The pre-treated CP was used as the working electrode. Pt-mesh and an Hg/HgO (0.1 M KOH) electrode were used as the counter and reference electrode, respectively. Electrodeposition of Ni-TEA film on CP was carried out at -1.7 V vs Hg/HgO for 5 min at room temperature. The final electrode was washed several times with ethanol and DI water and dried at room temperature for at least 12 hours. Meanwhile, Ni/CP-TEAx (x = 1, 3, 7, 9) was obtained by changing the TEA concentration in the deposition electrolyte to 1, 3, 7 and 9 mM. The Ni/CP sample was prepared using the same synthesis method but without the TEA electrolyte additive. To assess the impact of other additives, $NH_3 \cdot H_2O$, ethylenediaminetetraacetic acid (EDTA, $[CH_2N(CH_2CO_2H)_2]_2$) (5 mM) and ethanol were used instead of TEA as the electrolyte additive yielding samples named Ni/CP-NH_3, Ni/CP-EDTA and Ni/CP-Ethanol respectively.

Catalyst characterization

The field emission scanning electron microscopy (FESEM) images were obtained on a JEOL JSM-7001F microscope operating at 10 kV. Transmission electron microscopy (TEM) and energy dispersive X-ray (EDX) spectroscopy mapping studies were performed on a Hitachi HF5000 at an accelerating voltage of 60 kV with Oxford dual 100 mm^2 SDD EDX* detectors and a Hitachi HT7700 B operating at 80 kV. For TEM sample preparation, the electrocatalyst was scraped off the electrode surface and dispersed on the copper TEM grid (300 mesh). X-ray powder diffraction (XRPD) analysis was carried out on a Bruker D8 Advance MKII XRD using a Cu Kα radiation (λ = 1.54 Å). Fourier-transform infrared (FTIR) spectra were collected using a PerkinElmer Spectrum 100 FTIR spectrometer. X-ray photoelectron spectrometry (XPS) was measured using a Kratos Axis Supra+ XPS instrument with a monochromatic Al Kα X-ray source (1486.6 eV) and an Ag Lα X-ray source (2984.3 eV). The C 1s peak at 284.8 eV was used for binding energy charge-correction and CasaXPS software was used for XPS spectra analysis. For XPS depth profiling analysis, the sample was etched using an Ar ion cluster beam at a 5 keV beam energy and a 2 × 2 mm raster size. With these etching parameters, the etch rate was about 4 $nm \cdot min^{-1}$.

Electrochemical Measurements

Electrochemical tests were performed in a three-electrode setup connected to a BioLogic (VNP-300) potentiostat at room temperature. A Hg/HgO (0.1 M KOH) reference electrode and a Pt-mesh counter electrode were used. The as-prepared sample was used as the working electrode.

Linear sweep voltammetry (LSV) measurements were performed at 5 $mV \cdot s^{-1}$ in a 0.1 M KOH electrolyte. Four CV cycles were conducted before conducting the LSV. The potentials reported in this work are converted to the reversible hydrogen electrode (RHE) using the conversion equation: $E(\text{RHE}) = E(\text{Hg/HgO}) + 0.0591 \times \text{pH} + 0.165$ V, unless stated otherwise. All electrochemical experiments were done without iR-correction. The electrochemical surface area (ECSA) was measured by the double-layer capacitance (C_{dl}, mF) of the catalytic surface according to the equation ECSA = C_{dl}/C_s.[29] The C_{dl} was determined from scan-rate dependent cyclic voltammograms (CVs) at the non-Faradaic region, measured at scan rates of 20, 40, 60, 80, and 100 $mV \cdot s^{-1}$ between 0.1–0.2 V Hg/HgO. C_s is the specific capacitance value and the value of 0.04 $mF \cdot cm^{-1}$ was used in this work.[30] To evaluate the durability of the electrocatalyst, chronopotentiometric measurements were conducted at a constant current density of 10 $mA \cdot cm^{-2}$.

Results and Discussion

A simple electrodeposition procedure was used to prepare the Ni oxide electrocatalyst (Ni/CP-TEA), using a solution containing $NiSO_4 \cdot 6H_2O$ and triethanolamine (TEA) as the deposition electrolyte. Morphological analysis of the prepared samples was further conducted using field emission scanning electron microscopy (FESEM). As shown in Figure 1a and Figure S1a, the Ni/CP-TEA has a coral-like structure. The Ni/CP (Figure 1b) exhibits a rough surface made up of aggregated nanoparticles, averaging 1.07 ± 0.44 µm in size. X-ray diffraction (XRD) characterization was performed to explore the phase information of as-prepared samples. As shown in Figure 1c, the XRD pattern of the Ni/CP displays characteristic diffraction peaks corresponding to the {111} and {200} crystal planes of metallic Ni (PDF#01-071-4655) as well as those of the CP substrate. In contrast, no obvious Ni or NiO diffraction peaks can be observed in the pattern for the Ni/CP-TEA sample. This

could be due to a lower degree of Ni or NiO crystallinity or the CP substrate signals being too strong.

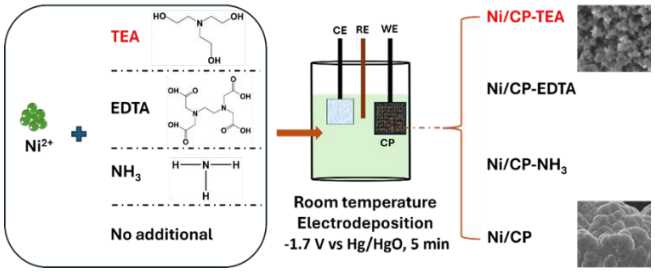

Scheme 1: A schematic illustration of the preparation of Ni/CP and Ni/CP-TEA, Ni/CP-EDTA and Ni/CP-NH_3 by adding TEA, EDTA and $NH_3{\cdot}H_2O$ in the Ni^{2+} solution, respectively.

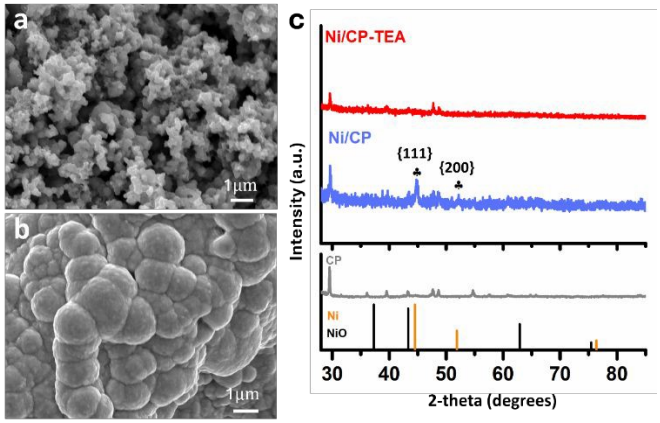

Figure 1. FESEM images of (a) Ni/CP-TEA and (b) Ni/CP. (c) XRD patterns of Ni/CP-TEA, Ni/CP and CP. NiO: PDF# 00-004-0835; Ni: PDF# 01-071-4655.

Transmission electron microscopy (TEM) was also performed to study the structure. The high-resolution TEM (HRTEM) image of Ni/CP-TEA (Figure S1b) reveals some lattice fringes (marked out by yellow circles), with very small domain sizes. The selected area electron diffraction (SAED) pattern (Figure S2a,b) displays diffuse diffraction rings, which confirms the small domain sizes. The diffraction rings are ascribed to NiO, indicating Ni oxidation when the electrode is exposed to air. Figure S2c exhibits the dark field STEM image of the Ni/CP-TEA and the related EDX elemental mapping of Ni and O showing uniform distribution of both elements.

The surface chemical composition of the as-prepared Ni/CP-TEA was analysed using XPS as shown in Figure 2a, in which the main peaks of Ni $2p_{3/2}$ and Ni $2p_{1/2}$ are displayed. Both Ni/CP-TEA and Ni/CP exhibit Ni^{2+} doublets, indicating the presence of a Ni oxide surface layer due to exposure to air post-synthesis. Additionally, small metallic Ni doublets (labelled Ni^0) are observed in the Ni/CP sample. The Ni^{2+} peak in the Ni/CP-TEA spectrum has a slightly lower binding energy than that of the Ni/CP (855.9 eV vs. 855.7, Ni $2p_{3/2}$). The positive shift indicates that the Ni^{2+} species in the Ni/CP-TEA have a lower electron density,[34] suggesting an electronic structure modification by TEA, which could influence the catalytic properties of the Ni/CP-TEA. This interaction can be verified by the N 1s spectra. As can be seen in Figure 2b, the N 1*s* signal is seen as a broad peak in the Ni/CP-TEA, showing features at 399.8 and 401.2 eV, attributed to metal-N (Ni-N) and O-N species,[35] respectively. In addition, the main peak at 399.8 eV is negatively shifted compared with that of the TEA (400.3 eV), further suggesting the coordination bond between TEA and the Ni, specifically with the N. As expected,

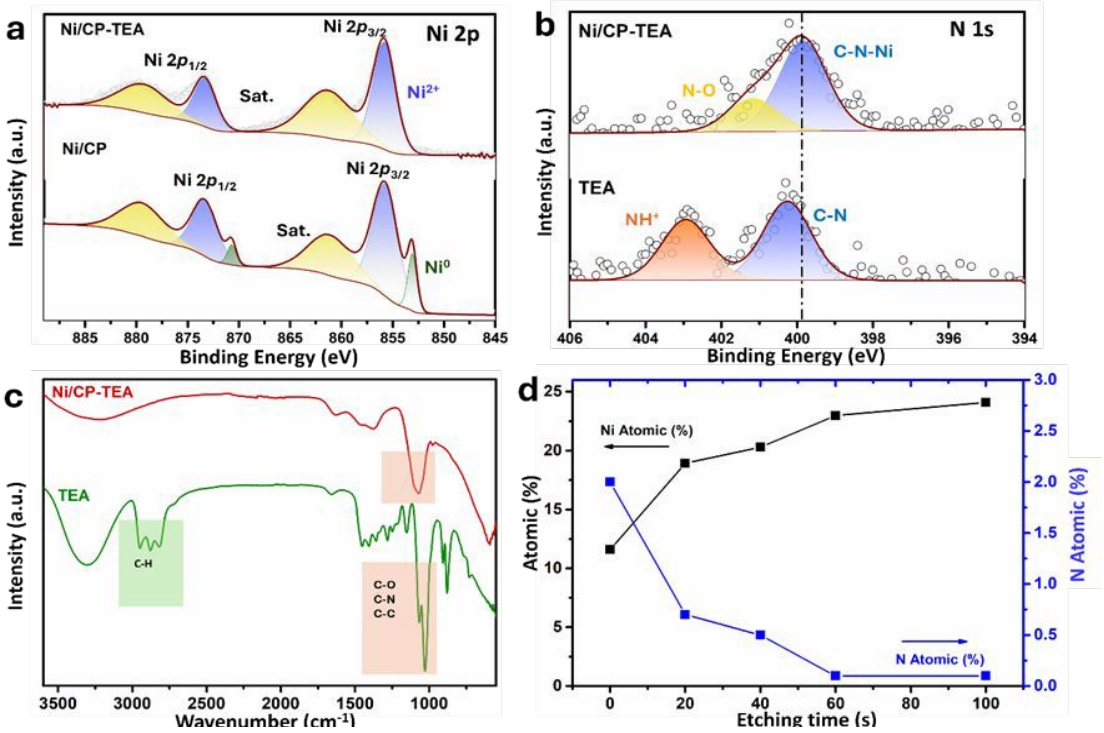

Figure 2. XPS spectra of (a) Ni 2*p* region of Ni/CP-TEA and Ni/CP; (b) N 1*s* region of Ni/CP-TEA and Ni/CP; (c) FTIR spectra of Ni/CP-TEA and TEA. (d) Surface N and Ni atomic concentration (at%; atom contains: C, N and O) as a function of etching time of Ni/CP-TEA from XPS depth profile analysis.

View Article Online
DOI: 10.1039/D4YA00430E

no N is detected in the Ni/CP (Figure S3).

This interaction is also verified through Fourier transform infrared (FTIR) spectroscopy of the Ni/CP-TEA, Ni/CP and TEA samples. As shown in Figure 2c, both the Ni/CP-TEA and the reference TEA samples have a typical broad band around 3300 cm^{-1}, which corresponds to the stretching vibration of the -OH groups.[31-33] Notably, the band peaks associated with C-H stretching and C-H bending in the region of 2814-2953 cm^{-1} and 880 cm^{-1} respectively,[36, 37] observed in TEA, cannot be detected in Ni/CP-TEA. The vibrational peaks attributed to C-N/C-C/C-O at around 1028 cm^{-1} in TEA, are detectable in the Ni/CP-TEA but show a blue shift of around 50 cm^{-1} (1070 cm^{-1}). The lack of the C-H peaks, coupled with the shift of the C-N/C-C/C-O peak, indicates an interaction between TEA and the Ni.[38, 39] For Ni/CP (Figure S4), no obvious band can be detected, indicating that the chemical environment of the Ni/CP-TEA is different to that of the Ni/CP.

To evaluate the N location in the Ni/CP-TEA, XPS depth profiling was measured with a total etch duration of 100 s (Figure 2d and Table S1). Before Ar^+ etching, the concentrations of Ni and N are 11.6 and 2.0 at%, respectively. During etching, the N content sharply decreased to a trace amount of 0.5 at% after 40 s, corresponding to an estimated etch depth of approximately 2.7 nm. This analysis indicates that the modification exists only at the surface of the Ni/CP-TEA.

The electrocatalytic performance of the samples for water oxidation was explored. A preliminary LSV test (Figure S5) was measured for the Ni/CP-TEAx prepared with different TEA concentrations (1, 3, 5, 7 and 9 mM). It shows that the optimal TEA concentration is 5 mM, exhibiting the highest OER activity, and so all Ni/CP-TEA samples subsequently discussed in this study were synthesized using 5 mM TEA. As shown in the LSV curve (Figure 3a), the Ni/CP-TEA requires a notably lower overpotential to reach the same current density than that of Ni/CP, demonstrating that the surface modification enhances OER activity. The bare CP substrate demonstrates negligible OER activity. The Ni/CP-TEA requires an overpotential (□) of about 320 mV to reach a current density of 10 $mA{\cdot}cm^{-2}$, which is considerably lower than that of Ni/CP (□ = 520 mV). This overpotential was determined from subsequent chronopotentiometry, where the overpotential stabilizes for the Ni/CP-TEA. This process is used as the Ni oxidation peak overlaps with the OER process, making it difficult to clearly separate the two in the preliminary LSV test.

The OER performance of the Ni/CP-TEA was also compared with various Ni-based electrocatalysts (Table S2). The Ni/CP-TEA exhibits a much lower overpotential (320 mV) to achieve a current density of 10 $mA{\cdot}cm^{-2}$ compared to the benchmark NiOx (430 mV) and is comparable to the active Ni-based electrocatalysts.

Trotochaud et al. reported that Fe impurities in KOH electrolyte could boost the OER activity of some Ni-based electrocatalysts by incorporation of Fe-impurities during CV or aging. This was demonstrated by the observations that the Fe 2*p* XPS signal could be detected even after 5 CV cycles and that the OER performance improved with each CV cycle.[40] To clarify the impact of Fe impurities on the Ni/CP-TEA, XPS spectra and CVs analysis were conducted. As shown in XPS spectra of Fe 2*p* region for the Ni/CP-TEA after stability test (Figure S6a), no Fe 2*p* signal can be detected. Additionally, in the

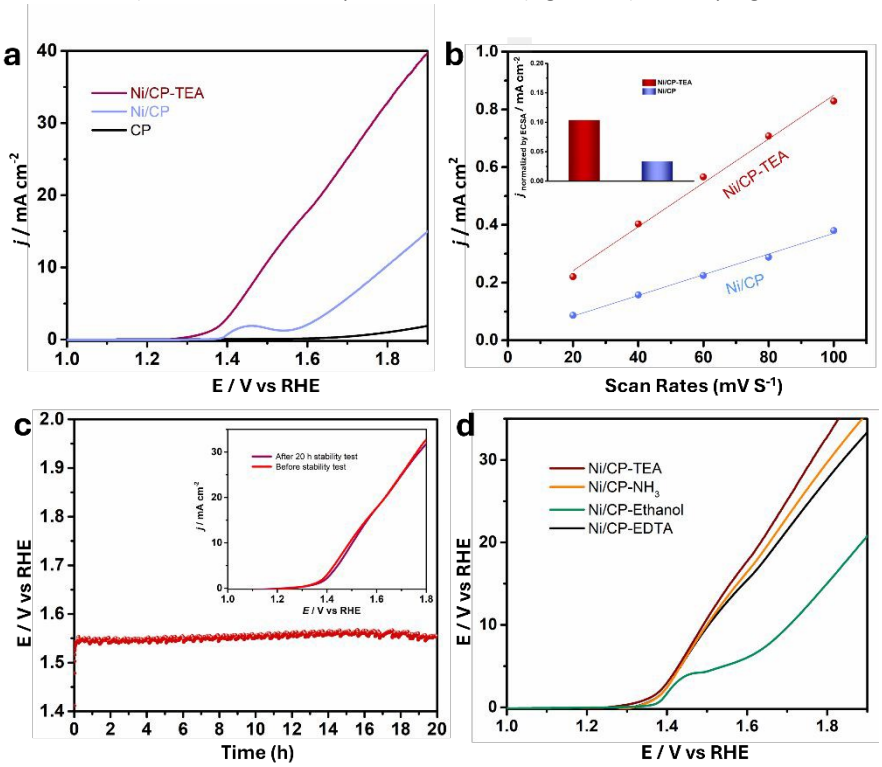

Figure 3. (a) Linear sweep voltammetry (LSV) polarization curve of Ni/CP-TEA, Ni/CP and CP at a scan rate of 5 $mV{\cdot}s^{-1}$ in 0.1 M KOH. (b) The ratio of current density against different scan rates based on the CV curves. Inset: Comparison of the current density normalized by the ECSA at overpotential of 400 mV. (c) Chronopotentiometry curve of Ni/CP-TEA at 10 $mA{\cdot}cm^{-2}$. The inset shows the LSV polarization curves of Ni/CP-TEA before and after the stability test. (d) LSV polarization curve of Ni/CP-TEA, Ni/CP-NH_3, Ni/CP-EDTA and Ni/CP-Ethanol at 5 $mV{\cdot}s^{-1}$ in 0.1 M KOH.

CV cycles (Figure S6b), it can be observed that the OER activity shows negligible change. These results indicate that the enhanced catalytic activity of the Ni/CP-TEA for OER cannot be attributed to Fe contamination.

To gain a better understanding of the catalytic OER activity, the electrochemical surface area (ECSA) was measured. The ECSA was evaluated using the electrochemical double-layer capacitance (C_{dl}). For the C_{dl} measurement, CV curves were recorded with different sweep rates (Figure S7). As shown in the Figure 3b, the C_{dl} values for Ni/CP-TEA and Ni/CP are 7.6 and 3.6 mF·cm^{-2}, respectively, demonstrating a larger ECSA and more active sites in the Ni/CP-TEA. This result is consistent with the coral-like structure in the Ni/CP-TEA (Figure 1a), in which more edges and surface area are exposed compared to the aggregated nanoparticles in the Ni/CP (Figure 1b).

To reveal the intrinsic OER activity, the LSV curves of the Ni/CP-TEA and Ni/CP were normalised against their ECSA and mass values (calculated based on the *I-t* curve of the electrodeposition process, as shown in Figure S8). The ECSA-normalised LSV curves (Figure S9) show that the Ni/CP-TEA possesses a significantly higher current density than the Ni/CP at the same potential, suggesting an enhancement in the intrinsic OER activity through TEA modification. As shown in the Figure 3b inset and Figure S10, at a given potential of 400 mV, the ECSA and mass normalised current density for the Ni/CP-TEA are 0.1 and 14.0 mA·cm^{-2}, respectively, which are 3.3 and 14 times higher than those of Ni/CP, respectively.

The long-term durability of the Ni/CP-TEA and Ni/CP samples was also measured in 0.1 M KOH. As shown in Figure 3c, the Ni/CP-TEA showed negligible potential change over 20 h at a current density of 10 mA·cm^{-2}(= 320 mV). Furthermore, the LSV curves before and after stability testing (inset of Figure 3c) also show negligible change. All the results demonstrate that the Ni/CP-TEA is an efficient OER electrocatalyst with high activity and good stability.

To verify whether the N or the -OH group in the TEA structure is primarily responsible for the observed effects and to assess whether other N-containing complex agents present similar effects, $NH_3{\cdot}H_2O$, ethylenediaminetetraacetic acid (EDTA) and ethanol were used as TEA substitutes. As shown in the Figure 3d, adding $NH_3{\cdot}H_2O$ and EDTA results in a similar OER activity increase, whereas adding ethanol only slightly increases OER performance. This indicates that the N group coordination is qualitatively responsible for the OER activity enhancement, rather than the -OH group. This also indicates that the use of surface modification with N group-containing ligands to enhance electrocatalytic OER activity can be expanded to other electrocatalysts.

To gain a deeper insight of the structure-function relationships and to understand the role of the N group in enhancing OER performance, the used electrodes were further characterized and compared to the as-prepared electrodes. As presented in Figure S11, the XRD patterns of the used and fresh Ni/CP-TEA are identical. Similarly, the XRD patterns of the used and fresh Ni/CP sample display similar diffraction peaks - assigned to Ni metal. The overall surface morphology (Figure S12) is preserved in both the used Ni/CP-TEA and Ni/CP. However, the used Ni/CP shows a smoother surface and a larger particle size (Figure S12b). In the TEM image (Figure 4a), the selected area electron diffraction (SAED) pattern only shows weaker diffraction rings ascribed to Ni oxide compared to the fresh sample. The structural reconstruction of Ni oxides under OER conditions can derive a large number of defects/vacancies, enhancing OER performance.[41, 42] The weaker diffraction rings and unchanged XRD profile observed in the used Ni/CP-TEA perhaps result from a lower degree of crystallinity with numerous defects/vacancies formed during the surface reconstruction under

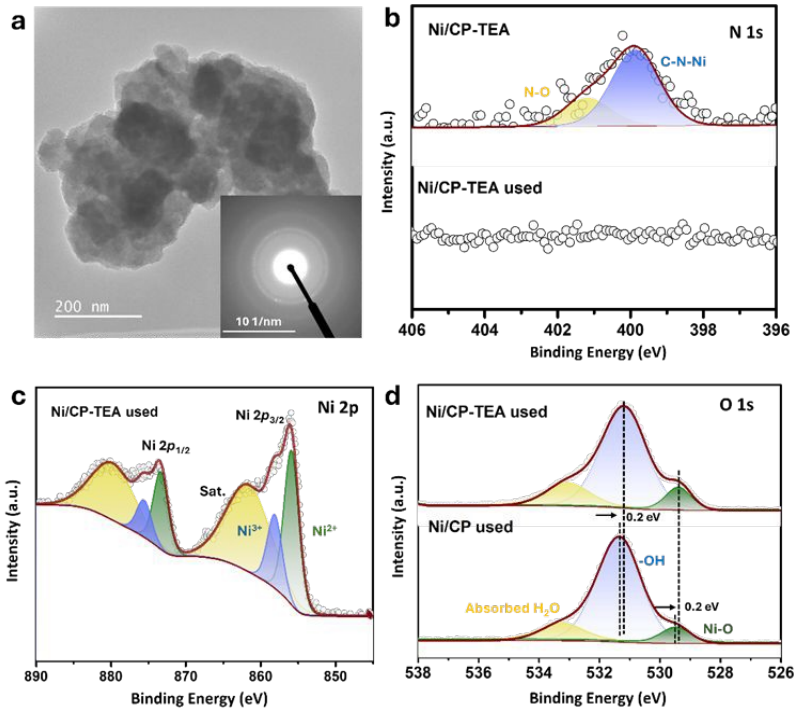

Figure 4. (a) HRTEM image of used Ni/CP-TEA (after LSV polarization curve) and the inset is the corresponding SAED pattern. (b) XPS spectra of N 1*s* region of fresh Ni/CP-TEA and used Ni/CP-TEA. (c) XPS spectrum of Ni 2*p* region of used Ni/CP-TEA. (d) XPS spectra of O 1*s* region of used Ni/CP-TEA and used Ni/CP.

OER condition, which could contribute to the enhanced activity. EDX mapping (Figure S13) of the used Ni/CP-TEA displays the distribution of Ni and O.

Further XPS analysis was conducted to analyze the surface chemical states of the used electrodes. As shown in Figure 4b, the N 1s signal cannot be detected in the used Ni/CP-TEA, suggesting the complete leaching of the N group from the surface of the used Ni/CP-TEA. Additionally, in the FTIR spectra (Figure S14), the vibrational peak corresponding to C-N/C-C/C-O presented in the fresh Ni/CP-TEA cannot be detected in the used sample, further confirming the complete dissociation of TEA in the used sample. The disappearance of N signal is accompanied by a shift in the Ni 2p XPS spectrum in the used Ni/CP-TEA. As shown in Figure 4c, for the used Ni/CP-TEA the Ni^{3+} species can be observed at 858.0 eV (Ni $2p_{3/2}$) and 875.5 eV (Ni $2p_{1/2}$). The Ni^{3+} species play a vital role for OER activity and are reported as the actual active center in the Ni-based electrocatalysts.[43] The For Ni/CP (Figure S15), the intensity of the Ni^0 peaks in the used Ni/CP is much lower than that of the fresh Ni/CP and the Ni^{2+} peaks remain well preserved. These results suggest that the *in-situ* leaching of TEA ligands induces the formation of high-valence Ni species in the Ni/CP-TEA. As for the O 1*s* spectra (Figure 4d), the used Ni/CP-TEA and used Ni/CP have the same components, whereas the O 1*s* peaks of the used Ni/CP-TEA shift negatively to a lower binding energy compared to those of the used Ni/CP. This negative shift demonstrates an increased electron density at the O atoms and indicates a higher Ni valence state in the Ni/CP-TEA, consistent with the Ni 2*p* XPS spectra.

Based on all experimental and characterization results presented in this study, the possible surface reconstruction and transformation process of the Ni/CP-TEA electrode during OER is presented in Figure 5. In the initial state, TEA interacts with surface Ni sites via coordination bonding between the N in TEA and the Ni. Under the anodic potential, the TEA ligands are completely leached. The Ni species on the surface are *in-situ* transformed into stable high-valent species, which finally serve as the OER-active sites. These high-valent Ni species endow the single-metal Ni oxide electrocatalyst with higher activity than the benchmark NiOx and make it comparable to other multi-metal and heteroatom doped OER electrocatalysts. This exemplifies the effect of N coordination bonding surface modification in accelerating the reconstruction process and facilitating the generation of stable active species for OER.

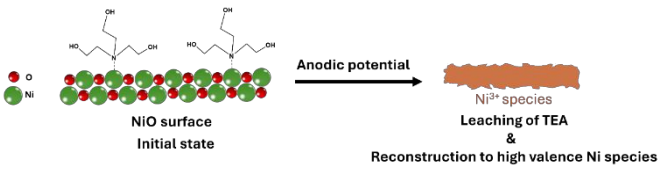

Figure 5. Proposed transformation of the electrode surface of Ni/CP-TEA during OER.

Conclusions

A N-group modified Ni electrocatalyst (Ni/CP-TEA) supported on a carbon paper substrate via a simple electrodeposition method has been fabricated, characterized and its performance as an OER electrocatalyst has been evaluated. The Ni/CP-TEA electrocatalyst displays enhanced OER performance, with an overpotential of 320 mV at 10 mA·cm^{-2} in 0.1 M KOH electrolyte, comparable to the best Ni-oxide based electrocatalysts reported to date for OER and shows good stability. The coral-like structure of the Ni/CP-TEA possesses larger surface area compared to the Ni/CP and more active sites for OER. The *in-situ* leaching of N group facilitates the rapid formation of high valence Ni species, specifically Ni^{3+}, thereby endowing the Ni/CP-TEA with enhanced OER activity. This work demonstrates the effect of modification of the Ni oxide surface with an N-group containing ligand to accelerate the rapid formation of high valence Ni species. This simple strategy may provide a new path for the low-cost and high-efficient design of OER electrocatalysts.

Author contributions

Jiayun Zhang: Conceptualization; Experiment; Formal analysis, Writing – original draft. Ruth Knibbe and Ian Gentle: Conceptualization, Supervision, Writing - review & editing, Funding acquisition.

Conflicts of interest

There are no conflicts to declare.

Acknowledgements

The work supported by The University of Queensland (UQ) and Australian Research Council through grants of DP200102573 and FT220100666. The authors gratefully acknowledge the use of facilities and the valuable technical assistance at the Centre for Microscopy and Microanalysis (CMM) facilities at The University of Queensland, Australia.

References

1. S. Chu, Y. Cui and N. Liu, *Nat Mater*, 2016, **16**, 16-22.
2. M. S. D. I. L. Thomas, *Nature*, 2001, **414**, 332–337
3. I. Staffell, D. Scamman, A. Velazquez Abad, P. Balcombe, P. E. Dodds, P. Ekins, N. Shah and K. R. Ward, *Energy & Environmental Science*, 2019, **12**, 463-491.
4. J. Turner, G. Sverdrup, M. K. Mann, P.-C. Maness, B. Kroposki, M. Ghirardi, R. J. Evans and D. Blake, *International Journal of Energy Research*, 2008, **32**, 379-407.
5. M. E. Lyons and S. Floquet, *Phys Chem Chem Phys*, 2011, **13**, 5314-5335.
6. T. Kwon, H. Yang, M. Jun, T. Kim, J. Joo, J. Kim, H. Baik, J. Y. Kim and K. Lee, *Journal of Materials Chemistry A*, 2021, **9**, 14352-14362.
7. J. Kibsgaard and I. Chorkendorff, *Nature Energy*, 2019, **4**, 430-433.
8. W. T. Hong, M. Risch, K. A. Stoerzinger, A. Grimaud, J. Suntivich and Y. Shao-Horn, *Energy & Environmental Science*, 2015, **8**, 1404-1427.
9. Y. P. Zhu, C. Guo, Y. Zheng and S. Z. Qiao, *Acc Chem Res*, 2017, **50**, 915-923.
10. M. S. Burke, L. J. Enman, A. S. Batchellor, S. Zou and S. W. Boettcher, *Chemistry of Materials*, 2015, **27**, 7549-7558.

11. F. Lu, M. Zhou, Y. Zhou and X. Zeng, *Small*, 2017, **13**.
12. S. Anantharaj, S. R. Ede, K. Sakthikumar, K. Karthick, S. Mishra and S. Kundu, *ACS Catalysis*, 2016, **6**, 8069-8097.
13. F. Song, L. Bai, A. Moysiadou, S. Lee, C. Hu, L. Liardet and X. Hu, *J Am Chem Soc*, 2018, **140**, 7748-7759.
14. K. Zhang and R. Zou, *Small*, 2021, **17**, e2100129.
15. Y. Li, X. Bao, D. Chen, Z. Wang, N. Dewangan, M. Li, Z. Xu, J. Wang, S. Kawi and Q. Zhong, *ChemCatChem*, 2019, **11**, 5913-5928.
16. M. Yu, E. Budiyanto and H. Tuysuz, *Angew Chem Int Ed Engl*, 2022, **61**, e202103824.
17. W. Yuan, C. Li, M. Zhao, J. Zhang, C. M. Li and S. P. Jiang, *Electrochimica Acta*, 2020, **342**.
18. M. Zhao, H. Li, W. Yuan and C. M. Li, *ACS Applied Energy Materials*, 2020, **3**, 3966-3977.
19. M. Gorlin, P. Chernev, J. Ferreira de Araujo, T. Reier, S. Dresp, B. Paul, R. Krahnert, H. Dau and P. Strasser, *J Am Chem Soc*, 2016, **138**, 5603-5614.
20. L. Gao, X. Cui, C. D. Sewell, J. Li and Z. Lin, *Chem Soc Rev*, 2021, **50**, 8428-8469.
21. S. Jin, *ACS Energy Letters*, 2017, **2**, 1937-1938.
22. H. Sun, X. Xu, Y. Song, W. Zhou and Z. Shao, *Advanced Functional Materials*, 2021, **31**.
23. H. Ding, H. Liu, W. Chu, C. Wu and Y. Xie, *Chem Rev*, 2021, **121**, 13174-13212.
24. D. Liu, H. Ai, J. Li, M. Fang, M. Chen, D. Liu, X. Du, P. Zhou, F. Li, K. H. Lo, Y. Tang, S. Chen, L. Wang, G. Xing and H. Pan, *Advanced Energy Materials*, 2020, **10**.
25. C. Huang, Q. Zhou, D. Duan, L. Yu, W. Zhang, Z. Wang, J. Liu, B. Peng, P. An, J. Zhang, L. Li, J. Yu and Y. Yu, *Energy & Environmental Science*, 2022, **15**, 4647-4658.
26. L.-M. Cao, J.-W. Wang, D.-C. Zhong and T.-B. Lu, *Journal of Materials Chemistry A*, 2018, **6**, 3224-3230.
27. L. An, J. Feng, Y. Zhang, R. Wang, H. Liu, G. C. Wang, F. Cheng and P. Xi, *Advanced Functional Materials*, 2018, **29**.
28. Y. Shi, Y. Yu, Y. Liang, Y. Du and B. Zhang, *Angew Chem Int Ed Engl*, 2019, **58**, 3769-3773.
29. E. Cossar, M. S. E. Houache, Z. Zhang and E. A. Baranova, *Journal of Electroanalytical Chemistry*, 2020, **870**.
30. M. Gao, W. Sheng, Z. Zhuang, Q. Fang, S. Gu, J. Jiang and Y. Yan, *J Am Chem Soc*, 2014, **136**, 7077-7084.
31. R. M. Zhaoping Liu, Minoru Osada, Kazunori Takada, and Takayoshi Sasaki, *Journal of the American Chemical Society*, 2005, **127**, 13869-13874.
32. D. P. Dubal, V. J. Fulari and C. D. Lokhande, *Microporous and Mesoporous Materials*, 2012, **151**, 511-516.
33. L. A. Saghatforoush, M. Hasanzadeh, S. Sanati and R. Mehdizadeh, *Bulletin of the Korean Chemical Society*, 2012, **33**, 2613-2618.
34. J. Hao, W. Luo, S. Wang, K. Zhao, J. Hou, L. Li, B. Ge, W. Yang and W. Shi, *Angew Chem Int Ed Engl*, 2021, **60**, 20042-20048.
35. J. Shen, X. Zheng, L. Peng, G. I. N. Waterhouse, L. Tan, J. Yang, L. Li and Z. Wei, *ACS Applied Nano Materials*, 2020, **3**, 11298-11306.
36. T. A. Mohamed, I. A. Shaaban, R. S. Farag, W. M. Zoghaib and M. S. Afifi, *Spectrochim Acta A Mol Biomol Spectrosc*, 2015, **135**, 417-427.
37. B. Song, C. Sizemore, L. Li, X. Huang, Z. Lin, K.-s. Moon and C.-P. Wong, *Journal of Materials Chemistry A*, 2015, **3**, 21789-21796.
38. A. Jawad, Y. Li, X. Lu, Z. Chen, W. Liu and G. Yin, *J Hazard Mater*, 2015, **289**, 165-173.
39. M. B. Jensen, S. Morandi, F. Prinetto, A. O. Sjåstad, U. Olsbye and G. Ghiotti, *Catalysis Today*, 2012, **197**, 38-49.
40. L. Trotochaud, S. L. Young, J. K. Ranney and S. W. Boettcher, *J Am Chem Soc*, 2014, **136**, 6744-6753.
41. R. Gao, M. Deng, Q. Yan, Z. Fang, L. Li, H. Shen and Z. Chen, *Small Methods*, 2021, **5**, e2100834.
42. T. Meng, Q. Li, M. Yan, D. Wang, L. Fan, X. Liu, Z. Xing and X. Yang, *Chemical Engineering Journal*, 2021, **410**.
43. Y. Liu, Z. Liu, L. Jia, D. Gao and Z. Tang, *Applied Surface Science*, 2022, **606**.

View Article Online
DOI: 10.1039/D4YA00420E

View Article Online
DOI: 10.1039/D4YA00420E

Triethanolamine-assisted surface reconstruction of nickel oxide for efficient oxygen evolution reaction

Jiayun Zhang [a], Ruth Knibbe [b] *, Ian Gentle [a] *

[a] School of Chemistry and Molecular Biosciences, The University of Queensland, Brisbane, QLD 4072, Australia

[b] School of Mechanical and Mining Engineering, The University of Queensland, Brisbane, QLD 4072, Australia

*Correspondence: ruth.knibbe@uq.edu.au; i.gentle@uq.edu.au

Data availability statements

The data supporting this article have been included as part of the Supplementary Information.